Design of haptic feedback control for Steer-by-Wire

Chugh, Tushar; Bruzelius, Fredrik; Klomp, Matthijs; Shyrokau, Barys

DOI
10.1109/ITSC.2018.8569795

Publication date
2018

Document Version
Final published version

Published in
Proceedings 2018 IEEE Intelligent Transportation Systems Conference (ITSC)

2018 21st International Conference on Intelligent Transportation Systems (ITSC)
Maui, Hawaii, USA, November 4-7, 2018

Design of Haptic Feedback Control for Steer-by-Wire*

Tushar Chugh[1], Fredrik Bruzelius[2], Matthijs Klomp[1] and Barys Shyrokau[3]

Abstract— **This paper illustrates a comparison of different haptic feedback control strategies; primarily focusing on open and closed-loop methods for a Force-Feedback Steer-by-Wire system. Due to shortcomings caused by the feedback motor impedance in the open loop architecture, the tracking performance is deteriorated. Consequently it is shown that the closed-loop solutions provide an improved response within the desired steering excitation range.**

The closed-loop possibilities, torque and position control, are designed and objectively compared in terms of performance and stability. The controller objectives are inertia compensation and reference tracking. For a given reference, the stability constraint between the controller gains responsible for the two objectives is contrasting in both the methods. Higher bandwidth is achieved for torque controller, whereas the driver arm inertia limits the position control performance. The linear system analysis is supported by the experimental results.

I. INTRODUCTION

With an increasing amount of driver support automated functions in a passenger car, the Steer-by-Wire (SbW) concept could be introduced in the near future. A typical hardware configuration consists of two actuators for controlling the road wheel and steering wheel respectively. This paper is about the latter, where the feedback motor is coupled to the steering wheel as a Human-Machine-Interface (HMI), also known as Force-Feedback (FF) system [1]. It eliminates the mechanical road coupling and relies on the steering feedback software. The challenge is integration of steering feedback software and automated functionality as mentioned in [2]. Keeping this motivation in context, the paper aims to present an unbiased comparison from haptic feedback (or steering feel) control viewpoint which could influence the interface design between them in hands-on/off situation.

Unlike the torque support provided in an Electric Power Assisted Steering (EPAS) system [3], [4], here the servo motor is responsible for creating the complete haptic feedback. In conventional steering systems with mechanical couping to the road, there are two sources of excitation; driver and external tire-road contact disturbance. The reference generator for SbW (refer [5], [6]) defining the haptic feedback is stated as the higher level control in the paper. An ideal higher level control should consider both the excitation sources to generate a realistic feedback, since it is an important part of the steering feel [3]. The road excitation is still an open question and a different domain in itself. This paper focuses on the feedback controller design using only driver excitation for a virtual feedback.

The higher level control algorithms presented by [5], [6] are implemented in an open loop configuration (direct feedback motor torque request). This compromises high frequency tracking performance. The question under investigation is to analyze the different haptic feedback control strategies and quantify their improvement potential. For closed-loop methods, a lower level controller is introduced with the feedback control law acting on the higher level request. As a consequence, the proposed control architecture exhibits a cascade structure similar to [7], [8]. The inner loop minimizes the error in the control variable, whereas the outer loop ensures generation of the reference variable, see for example [7], [8], [9]. There are two possibilities: torque and position control; also known as impedance and admittance control respectively [10]. The position control approach categorizes the concept of controlling one of the motion states. It could also be defined as a velocity controller. The definition is made on the basis of feedback control variable. The research in [11], [12] proposed a hybrid controller, which by the definition applied in this paper would categorize them under position/velocity controller. The higher level control is designed to provide a good steering feel, while the lower level control aims to track it.

In biomechanics [8], [11], the stability and performance are studied for the higher level control (to design the reference parameters) given the lower level control. This paper considers the higher level control to be given. And the stability criteria and performance are discussed for the lower level control (or feedback control law) using linear system analysis. Furthermore, the human coupled interaction with the haptic controller (in terms of driver's muscular arm properties) is discussed to highlight the fundamental differences between the two approaches.

II. SYSTEM DYNAMICS AND IDENTIFICATION

A. Force-Feedback (FF) System and Driver Arm Mechanics

A FF-system (further stated as plant model) is an HMI where the feedback motor interacts with the driver via torsion bar compliance, refer Fig. 1. The purpose is to generate the required steering torque feedback. Linear plant

*The research activities have been performed as a part of the ITEAM project in the European Union's Horizon 2020 research and innovation program under Marie Sklodowska-Curie Grant Agreement No. 675999.

[1]Tushar Chugh and Matthijs Klomp are with Chassis Strategy & Concept Department at Volvo Car Corporation and Chalmers University of Technology, Gothenburg, Sweden tushar.chugh@volvocars.com; matthijs.klomp@volvocars.com

[2]Fredrik Bruzelius is with VTI (Swedish National Road and Transport Research Institute) and Mechanics & Maritime Sciences Department at Chalmers University of Technology, Gothenburg, Sweden fredrik.bruzelius@chalmers.se

[3]Barys Shyrokau is with Intelligent Vehicles group at the Department of Cognitive Robotics, Delft University of Technology, Delft, The Netherlands barys.shyrokau@tudelft.nl

TABLE I
DESCRIPTION OF VARIABLES, NOTATIONS AND PARAMETERS

Name	*Description*	*Name*	*Description*
M_{arm}	Muscular arm torque (Nm)	$\theta_{s,req}$	Steering wheel angle request (rad)
M_{tb}	Torsion bar torque (Nm)	θ_s	Steering wheel angle (rad)
$M_{tb,ref}$	Reference torsion bar torque (Nm)	θ_{mot}	Motor angle (rad)
M_{mot}	Motor torque (Nm)	$\theta_{mot,ref}$	Reference motor angle (rad)
M_s	Steering wheel torque (Nm)	θ_{pin}	Pinion angle (rad)
k_{arm}	Driver arm damping (Nms/rad)	b_s	Steering viscous damping (Nms/rad)
k_{tb}	Torsion bar damping (Nms/rad)	b_{mot}	Motor viscous damping (Nms/rad)
k_{ref}	Reference damping (Nms/rad)	ω	Frequency (rad/s)
c_{arm}	Driver arm stiffness (Nm/rad)	D	Damping ratio (-)
c_{tb}	Torsion bar stiffness (Nm/rad)	t	Time domain operator
c_{ref}	Reference stiffness (Nm/rad)	s	Laplace operator
J_s	Steering wheel inertia (kgm^2)	v_x	Longitudinal vehicle speed (m/s)
J_{mot}	Motor inertia (kgm^2)	T_f	Filter time constant (s)
J_{arm}	Driver arm inertia (kgm^2)	G_i, L_i	Transfer functions
J_{ref}	Reference inertia (kgm^2)	K_i	Feedback gains

is considered without Coulomb friction. Because for high input amplitudes and excitation frequencies, this is a valid assumption [13]. Equation (1), (2) and (3) represent system (or plant) dynamics in time domain.

The driver arm inertia, J_{arm}, is reasonably assumed rigidly coupled to the steering wheel [14], such that $J_{arm}\ddot{\theta}_s(t) = M_{arm}(t) - M_s(t)$. As a result the controller bandwidth depends on it, further discussed below. Human applies force/torque to a mechanical system and position becomes the feedback [15]. Therefore, the plant considers M_{arm} as the primary input. Equation (4) represents the driver's arm muscle co-contraction (as an actuator). The parameters muscular intrinsic stiffness, damping and arm inertia are taken from [14]. The motor current controller and sensors (for angle and torque) have fast dynamics, such that the bandwidth is much higher than the controller. Hence, they are assumed as unit transfer functions.

$$J_s\ddot{\theta}_s(t) + b_s\dot{\theta}_s(t) = M_s(t) - M_{tb}(t) \tag{1}$$

$$J_{mot}\ddot{\theta}_{mot}(t) + b_{mot}\dot{\theta}_{mot}(t) = M_{tb}(t) - M_{mot}(t) \tag{2}$$

$$k_{tb}(\dot{\theta}_s(t) - \dot{\theta}_{mot}(t)) + c_{tb}(\theta_s(t) - \theta_{mot}(t)) = M_{tb}(t) \tag{3}$$

$$k_{arm}(\dot{\theta}_{s,req}(t) - \dot{\theta}_s(t)) + c_{arm}(\theta_{s,req}(t) - \theta_s(t)) = M_{arm}(t) \tag{4}$$

B. Experimental Setup

The FF-system consists of steering wheel actuated using a direct drive brushless DC-motor with an external torque sensor mounted between the steering wheel and servo motor

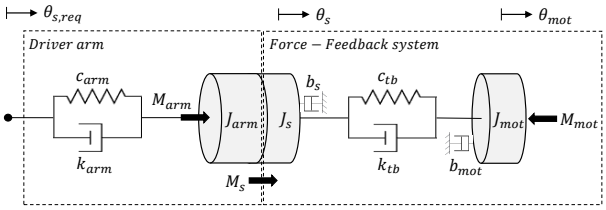

Fig. 1. Block diagram of FF-system and driver arm mechanics. The plant overall has 2-DOF; steering wheel angle and feedback motor angle.

input shaft. The feedback motor has a rated torque of 7.5Nm with a resolution of 0.03Nm. The motor angle resolution is 0.009° incremental. The communication between the FF-system and dSPACE real-time (DS1006) machine is realized via CAN interface at 1kHz. During experiments, the motor torque saturation limit was maintained at all times.

C. Data Post-processing

Frequency response data analysis has been done as explained in [16]. The linear time invariant (LTI) transfer function estimate is defined as the ratio of output-input cross spectral and input spectral estimates. Consequently, for lower noise interference 95% coherence spectrum criteria is fixed.

D. System Identification

The parameters feedback motor inertia, J_{mot}, and viscous damping, b_{mot}, are unknown. It is important to quantify them for the development and validation of the control strategy. System identification is employed for parameter estimation. At first, the passive FF-steering is excited by the driver such that $M_{mot}(t) = 0$. The resulting relationship between the torsion bar torque to motor angle becomes (5) in Laplace domain. From the frequency response data, the transfer function is estimated using the weighted least square criterion for the linear regression on gain and phase as shown in Fig. 2(a). These parameters are further validated by setting up the motor torque with a reference, $M_{mot}(t) = c_{ref}\theta_{mot}(t) + k_{ref}\dot{\theta}_{mot}(t)$. The resulting transfer function (6) as shown in Fig. 2(b) is obtained with driver excitation. Lastly, the validation is done by motor excitation with a low amplitude disturbance signal in hands-off condition. The transfer function is same as (5), but with motor torque in the denominator and -1 in the numerator, refer Fig. 2(c).

$$\frac{\theta_{mot}(s)}{M_{tb}(s)} = \frac{1}{J_{mot}s^2 + b_{mot}s} \tag{5}$$

$$\frac{M_{tb}(s)}{M_{mot}(s)} = 1 + \frac{J_{mot}s^2 + b_{mot}s}{k_{ref}s + c_{ref}} \tag{6}$$

III. HAPTIC FEEDBACK CONTROL STRATEGIES

In this section, the steering feel reference is introduced at first which primarily defines the open loop architecture. Then the problem formulation is covered in the open loop explanation. Finally the closed-loop solutions, torque and position control, are designed analytically and then evaluated in simulation before the experiments and comparison.

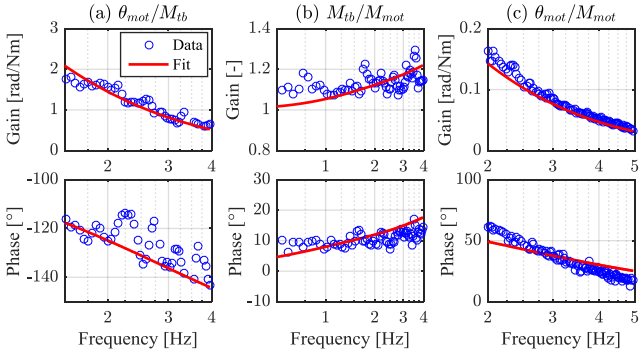

Fig. 2. System identification results from 3 test cases for estimation of parameters J_{mot} and b_{mot}. (a) Frequency response of torsion bar torque to motor angle for a passive system ($M_{mot} = 0$) with driver excitation. (b) Frequency response of motor torque to torsion bar torque with a known reference and driver excitation. (c) Frequency response of motor torque to motor angle with external motor torque excitation in hands-off condition.

A. Reference

The haptic feedback is generated with virtual dynamics in the higher level control. Since the system is mechanically decoupled from the road contact, the reference defines the desired response (consisting of stiffness, damping and inertia). The steering feel reference is objectified in terms of torsion bar torque to pinion angle for a state-of-the-art EPAS system using open loop maneuvers as described in [17]. The same reference has been implemented for the closed-loop EPAS in [18]. The difference between an EPAS and SbW is downstream of the torque sensor. The upstream architecture which includes driver arms, steering wheel, etc. is the same. Hence, the control reference is selected at the torque sensor where both signals, torque and angle, are measurable. The driver arm's muscular admittance is time-variant [19]. However, the controllers are designed by coupling the arms to the steering wheel with high muscle co-contraction as the worst case. The linearized reference is already given for a vehicle speed of 75km/h assuming a good steering feel representation. This function only models the driver-side of the steering excitation. The external road disturbance source is not included. The resulting reference transfer function is given in (7). The two eigenfrequencies correspond to vehicle yaw ($\approx$1$-$2Hz) and pinion dynamics ($\approx$2$-$3Hz), refer [17], [20]. The reference function is proper because torsion bar torque acts as an input and pinion angle as an output. As a result, the reference inverse is improper and therefore requires a second-order filter as shown in (8), further discussed in detail. The reference and reference inverse are required for the higher level control. The same higher level control in [18] signifies that the EPAS pinion angle must be equivalent to the SbW feedback motor angle, $\theta_{mot}(t) \equiv \theta_{pin}(t)$.

$$G_{ref} = \frac{\theta_{pin}(s)}{M_{tb}(s)} = \frac{b_2 s^2 + b_1 s + b_0}{a_4 s^4 + a_3 s^3 + a_2 s^2 + a_1 s + a_0} \tag{7}$$

$$G_{ref}^{-1} = \frac{M_{tb}(s)}{\theta_{pin}(s)} = \frac{1}{G_{ref}} \frac{\omega_f^2}{s^2 + 2D_f\omega_f s + \omega_f^2} \tag{8}$$

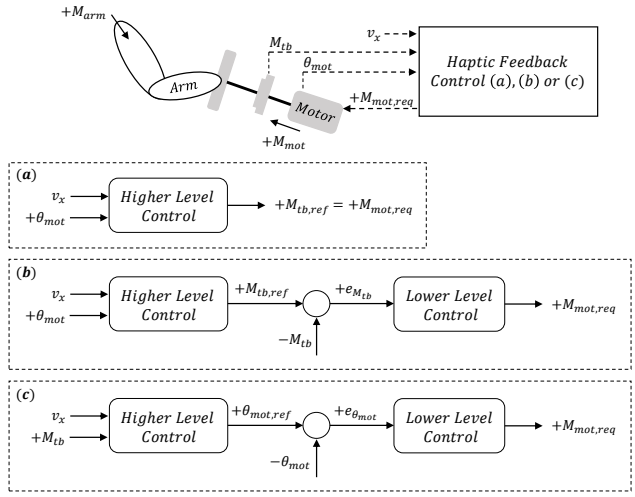

Fig. 3. Haptic feedback control for SbW FF-system. (a) Open loop: Reference inverse as the higher level control and no feedback control. (b) Torque control: Reference inverse and torsion bar torque feedback as the higher and lower level control respectively. (c) Position control: Reference and motor angle feedback as the higher and lower level control respectively.

B. Open Loop

The straightforward FF-steering architecture is open loop where the feedback motor angle (or angular position) computes the reference torque, refer Fig. 3(a). Typically, the higher level control represents a vehicle model [6] with empirical steering feel functions [5]. Using reference inverse (8) as the higher level control, the reference torsion bar torque (9) is requested to the feedback motor.

$$M_{tb,ref}(s) = G_{ref}^{-1}\theta_{mot}(s) \tag{9}$$

Equation (2) is important for the haptic feedback control because it couples the virtual environment to mechanical hardware. Transforming (2) to Laplace domain, the reference haptic feedback function is derived in (10). It should ideally be close to unity within the driver's periodic steering excitation range (up to 4$-$5Hz) [21]. Using (9) and (10), the reference tracking performance is defined in terms of torsion bar torque to motor angle (or angular velocity) as (11). Due to motor inertia and viscous damping, the haptic feedback deteriorates at higher frequencies. The compromised (open loop) tracking performance (with respect to given reference) is shown in Fig. 6(a) and (b), frequency response of torsion bar torque to motor angle and angular velocity respectively. Also, Fig. 6(c) represents the problem more objectively based on the frequency response of reference to actual torsion bar torque (deviating from unity at frequencies greater than 2Hz).

$$\frac{M_{tb}(s)}{M_{mot}(s)} = \frac{M_{tb}(s)}{M_{tb,ref}(s)} = 1 + \frac{J_{mot}s^2 + b_{mot}s}{G_{ref}^{-1}} \tag{10}$$

$$\frac{\theta_{mot}(s)}{M_{tb}(s)} = \frac{1}{(J_{mot}s^2 + b_{mot}s) + G_{ref}^{-1}} \tag{11}$$

The loop transfer function, L_O, determines the characteristic equation and subsequently ensures a stable coupling of

the haptic feedback control to the plant model, refer (12). The 'plant' transfer function signifies the passive model behavior obtained using (1)−(3). For the given reference, the phase margin is used to design the reference inverse filter as mentioned in (8). The selected filter time constant, $T_f = 5$ms (or cut-off frequency $\omega_f = 200$rad/s), with critical damping ratio provides 45° phase margin for L_O.

$$G_{char,O} = 1 + L_O : L_O = -G_{ref}^{-1} \left| \frac{\theta_{mot}(s)}{M_{mot}(s)} \right|_{plant} \tag{12}$$

C. Torque Control

The closed-loop torque control architecture requires the same higher level control as in open loop along with a lower level (or feedback) control function, $G_{Fb,M}$, as shown in Fig. 3(b). The strategy has been termed on the basis of control error in torsion bar torque. The reference torque (9) is requested to the lower level control. The control objective is to improve reference tracking by compensating the feedback motor impedance. The lower level control has been designed independent of the higher level control with fast response keeping a desired stability margin. Considering (2), the motor torque request, reference haptic feedback and tracking transfer functions are given as follows respectively.

$$M_{mot}(s) = G_{Fb,M}(M_{tb,ref}(s) - M_{tb}(s)) \tag{13}$$

$$\frac{M_{tb}(s)}{M_{tb,ref}(s)} = \frac{(J_{mot}s^2 + b_{mot}s) + G_{ref}^{-1}G_{Fb,M}}{G_{ref}^{-1}(1 + G_{Fb,M})} \tag{14}$$

$$\frac{\theta_{mot}(s)}{M_{tb}(s)} = \frac{1 + G_{Fb,M}}{(J_{mot}s^2 + b_{mot}s) + G_{ref}^{-1}G_{Fb,M}} \tag{15}$$

The feedback control law is derived using lower and upper bounds. The lower bound in (16) replicates the open loop behavior assuming an infinitely stiff torsion bar, such that $J_{sys} = J_{arm} + J_s + J_{mot}$ and $b_{sys} = b_s + b_{mot}$. Whereas the upper bound is obtained by assuming a desired controller bandwidth as first-order transfer function, $G_{des} = 1/(1 + T_f s)$.

$$\begin{aligned} G_{Fb,M}\big|_{lower} &= \frac{-G_{ref}^{-1}}{J_{sys}s^2 + b_{sys}s} \\ G_{Fb,M}\big|_{upper} &= \frac{G_{des}}{(1 - G_{des})\left|\frac{M_{tb}(s)}{M_{mot}(s)}\right|_{plant}} \end{aligned} \tag{16}$$

The above derived bounds analytically indicates an ideal torque control law. As seen in Fig. 4(a), the integrator is a necessary requirement because there is no stiffness in the system. This is due to the plant pole at the origin from motor torque to motor angle. Hence an integral gain, $K_{i,M}$, eliminates the steady state error and ensures transient tracking. The closed-loop LTI system remains both reachable and observable (for motor angle on the outer loop) with integral controller since there are no pole/zero cancellations, see [9], [22].

For a simplified analytical explanation, the reference inverse is assumed as a second-order (inertia-spring-damper) model in (17). Using the final value theorem for an angular step disturbance, $\Delta\theta_{dist}$ (at $t = 0$), results in steady state torque (18), for given reference inverse and integral controller ($G_{Fb,M} = K_{i,M}/s$). For minimum steady state error, $K_{i,M}$ (>0) should be higher. Higher $K_{i,M}$ also results in higher controller bandwidth but at the expense of gain margin. The final control law also includes a proportional gain, $K_{p,M}$, such that $G_{Fb,M} = K_{i,M}/s + K_{p,M}$. The motor impedance is effectively reduced by a factor of $(1 + K_{p,M})$, $\forall\ K_{p,M} > 0$ [23]. This can be seen in (19) using the initial value theorem on (14) for a step reference torque disturbance, ΔM_{dist} (at $t = 0$).

$$G_{ref}^{-1} = J_{ref}s^2 + b_{ref}s + c_{ref} \tag{17}$$

$$\Delta M_{tb} = \lim_{s\to 0} \frac{M_{tb}(s)}{\theta_{mot}(s)} \Delta\theta_{dist} = \lim_{s\to 0} c_{ref}\Delta\theta_{dist} \left[\frac{1}{1 + \frac{s}{K_{i,M}}} \right] \tag{18}$$

$$\Delta M_{tb} = \lim_{s\to \infty} \frac{M_{tb}(s)}{M_{tb,ref}(s)} \Delta M_{dist} = \Delta M_{dist} \left[\frac{\frac{J_{mot}}{J_{ref}} + K_{p,M}}{1 + K_{p,M}} \right] \tag{19}$$

The controller is developed in a sequential manner as described in [18]. At first, the inner loop stability criteria is satisfied for the loop transfer function (20) if the constraint (21) holds true, where $\alpha = 1 + K_{p,M}$. This is a necessary and sufficient stability condition for the characteristic equation ($G_{char} = 1 + L$), excluding the reference inverse to have LHP closed-loop poles. The condition has been verified numerically for a stiff torsion bar (as an approximation) because as c_{tb} reduces $K_{i,M}$ upper bound increases. The inner loop stability and performance primarily depends on the torsion bar and motor viscous damping. Removing the torsion bar demands a robust estimated torque signal for the closed-loop approach because the stability limit is dependent on it. On the contrary, lower magnitude of $K_{i,M}$ and $K_{p,M}$ is undesirable for higher bandwidth. In the given setup they are selected to achieve infinite gain margin, 35° phase margin for (20) and 12Hz torque controller bandwidth.

$$L_{in,M} = G_{Fb,M} \left| \frac{M_{tb}(s)}{M_{mot}(s)} \right|_{plant} \tag{20}$$

$$K_{i,M} < \left[\alpha + \frac{J_{mot}}{J_s + J_{arm}} \right]^2 \frac{k_{tb}}{J_{mot}} + \alpha \frac{b_{mot}}{J_{mot}} + \frac{J_{mot}b_s}{(J_s + J_{arm})^2} \tag{21}$$

The next step is to include the outer loop (with higher level control). The loop transfer function becomes (22). With known reference stiffness, c_{ref}, and inner loop bandwidth, ω_{in}, the sufficient closed-loop stability condition is to have no loop gain encirclements of -1 (Nyquist criterion). It yields in (23) with reasonable assumptions, $\{J_{ref}, b_{ref}, k_{tb}\} = 0$ and $c_{tb} \to \infty$. This condition is satisfied for the given parameters. With the defined control law, (22) has 32° phase margin.

$$L_{o,M} = G_{Fb,M} \left[\left| \frac{M_{tb}(s)}{M_{mot}(s)} \right|_{plant} - G_{ref}^{-1} \left| \frac{\theta_{mot}(s)}{M_{mot}(s)} \right|_{plant} \right] \tag{22}$$

$$\omega_{in} > \frac{c_{ref}}{b_s} - \frac{b_s}{J_s + J_{arm}} \tag{23}$$

The coupled stability of a haptic controller ultimately depends on its interaction with the environment, considering

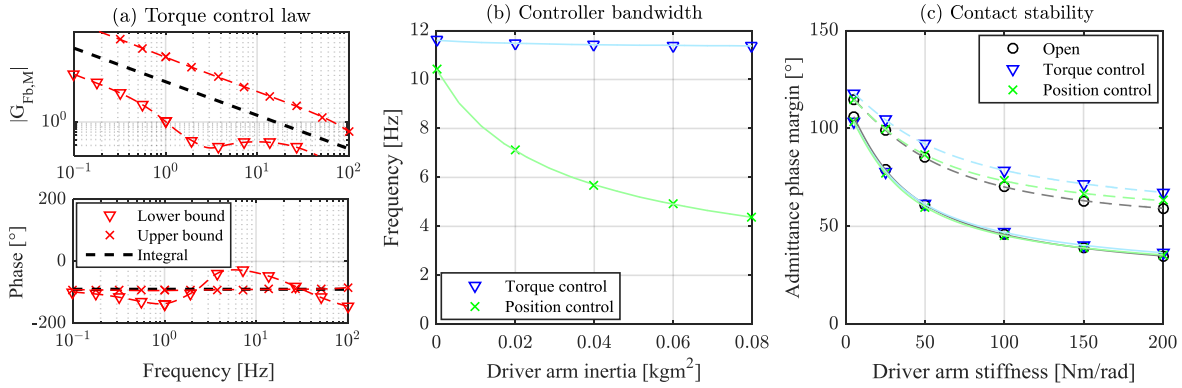

Fig. 4. (a) Torque feedback control transfer function ($G_{Fb,M}$) as an integrator ($K_{i,M}/s$), also with lower and upper bounds as defined in (16). The lower bound function replicates the open loop result assuming stiff torsion bar. Whereas the upper bound function defines a desired torque controller bandwidth ($\omega_{in} = 1/T_f$), represented by G_{des}. (b) It shows the influence of driver arm inertia (J_{arm}) on torque and position controller bandwidth using their defined control laws. Torque controller bandwidth (12Hz) is almost independent of J_{arm} variation, but the bandwidth varies noticeably in position controller (from 10Hz to 4Hz without and with maximum J_{arm} respectively). (c) Coupled or contact stability is defined for the loop transfer function (24). The respective admittance phase margin variation as a function of driver arm stiffness (c_{arm}) is shown here for $J_{arm} = 0$ (dashed lines) and $J_{arm} \neq 0$ (solid lines).

driver/human-in-the-loop. The instability of haptic manipulators is often termed as contact instability, see [23], [24]. The environment stiffness is primarily defined by the driver arm inertia, J_{arm}, and muscular arm stiffness (or co-contraction), c_{arm}. The effect of J_{arm} variation marginally influences the torque controller bandwidth (refer Fig. 4(b)), inner- and outer-loop phase margins. Secondly, the effect of c_{arm} variation is understood by coupling the driver arm's intrinsic stiffness and damping ($G_{arm}^{-1} = c_{arm} + k_{arm}s$) with closed-loop steering admittance, $\theta_s(s)/M_{arm}(s)$. Equation (24) is the resulting loop transfer function. Following the above mentioned design approach and satisfying the constraints ensure positive real closed-loop admittance. This is a necessary and sufficient stability condition (for a stable LTI plant) coupled to a stable and passive environment [23]. Fig. 4(c) exhibits the effect of c_{arm} variation on admittance phase margin. Higher driver arm inertia and stiffness results in decreasing phase margin. But the admittance poles still remain in LHP for the root locus plot ensuring coupled stability.

$$L_d = G_{arm}^{-1} \left| \frac{\theta_s(s)}{M_{arm}(s)} \right|_{closed} \tag{24}$$

Using the same control law, the controller stability was maintained during experiments (for both hands-off and rigidly coupled hands-on). With driver excitation, the reference tracking of torsion bar torque to motor angle and angular velocity is significantly improved as compared to the open loop architecture, refer Fig. 6(a) and (b). Because the reference haptic feedback function stays close to unity within the steering excitation range as shown in Fig. 6(c).

D. Position Control

The closed-loop position controller requires reference in (7) as the higher level control. The lower level control as shown in Fig. 3(c) acts as an angular position error feedback. The reference motor angle, $\theta_{mot,ref}(s) = G_{ref} M_{tb}(s)$, is requested to the lower level control. The control objective is same as before to improve reference tracking. Considering (2) and postion feedback function as $G_{Fb,\theta}$, the motor torque request, reference haptic feedback and tracking transfer functions become as follows respectively.

$$M_{mot}(s) = G_{Fb,\theta}(\theta_{mot,ref}(s) - \theta_{mot}(s)) \tag{25}$$

$$\frac{\theta_{mot}(s)}{\theta_{mot,ref}(s)} = \frac{1 - G_{ref}G_{Fb,\theta}}{G_{ref}((J_{mot}s^2 + b_{mot}s) - G_{Fb,\theta})} \tag{26}$$

$$\frac{\theta_{mot}(s)}{M_{tb}(s)} = \frac{1 - G_{ref}G_{Fb,\theta}}{(J_{mot}s^2 + b_{mot}s) - G_{Fb,\theta}} \tag{27}$$

The position feedback control law is derived using torque control, $G_{Fb,M} = K_{i,M}/s + K_{p,M}$, similar to [18]. For a similar performance as torque controller (in terms of reference tracking), the respective closed-loop characteristic equations are compared $G_{char,M} \stackrel{!}{=} G_{char,\theta}$, where $G_{char,M} = 1 + L_{o,M}$. The result is shown in (28). Using (17) and $G_{Fb,M}$, the position feedback control transfer function can be written as (29). The feedback gains ($K_{d2,\theta}, K_{d,\theta}, K_{p,\theta}$ and $K_{i,\theta}$) are selected independent of reference parameters to have fast inner loop response with a desired stability margin. The derived position feedback control law consists of higher order derivatives to manipulate the haptic feedback. For a similar haptic performance theoretically (as in torque control), here the control objective is to minimize the error in motor angular position, velocity and acceleration simultaneously. In torque control the higher level control (8) requires filtering, whereas the filtering is done in the position feedback control (for derivative and double-derivative terms). For a fair comparison, the same filter is used in both. The closed-loop LTI system remains fully reachable and observable (with torsion bar torque on the outer loop) without any pole/zero cancellations.

$$G_{Fb,\theta} = -G_{Fb,M}G_{ref}^{-1} \tag{28}$$

$$G_{Fb,\theta} = -(K_{d2,\theta}s^2 + K_{d,\theta}s + K_{p,\theta} + K_{i,\theta}/s) \tag{29}$$

The inner loop is a position controller which is developed at first to minimize the control error in motor

angle based on (29). The controller development is inspired from [25], [18]. For a simplified explanation, consider (2) as the plant model with infinitively stiff torsion bar such that the plant transfer function becomes $\theta_{mot}(s)/M_{mot}(s) = -1/(J_{sys}s^2 + b_{sys}s)$, where $J_{sys} = J_{arm} + J_s + J_{mot}$ and $b_{sys} = b_s + b_{mot}$. Given feedback control function, $G_{Fb,\theta}$, the closed-loop reference and disturbance transfer functions are (30) and (31) respectively.

$$\frac{\theta_{mot}(s)}{\theta_{mot,ref}(s)} = \frac{-G_{Fb,\theta}}{J_{sys}s^2 + b_{sys}s - G_{Fb,\theta}} \tag{30}$$

$$\frac{\theta_{mot}(s)}{M_{dist}(s)} = \frac{-1}{J_{sys}s^2 + b_{sys}s - G_{Fb,\theta}} \tag{31}$$

The required controller bandwidth and damping are achieved using the proportional and derivative gains, $K_{p,\theta}$ and $K_{d,\theta}$ respectively. Assuming $G_{Fb,\theta} = -(K_{d,\theta}s/(1 + T_f s) + K_{p,\theta})$, the resulting loop gain, $L(j\omega)$, is shown in (32). For $\{K_{d,\theta}, T_f\} = 0$, increasing $K_{p,\theta}$ results in higher bandwidth ($\omega_{in} = \sqrt{K_{p,\theta}/J_{sys}}$) but the damping ($D_{in} = b_{sys}/2J_{sys}\omega_{in}$) reduces which ultimately affects the phase margin. Improvement in phase margin is attained by increasing $K_{d,\theta}$. With $T_f = 5$ms, the effect of $K_{p,\theta}$ and $K_{d,\theta}$ variation on controller bandwidth and phase margin can be seen in Fig. 5 for two load cases, with and without J_{arm}. The influence of arm inertia variation noticeably alters the controller performance and phase margin. For instance if $K_{p,\theta} = 30$ and $K_{d,\theta} = 2$, with higher system inertia the bandwidth and phase margin reduces by 7Hz and 10° respectively. Moreover, the integral gain, $K_{i,\theta}$, is required to minimize the steady state error and attenuate external load torque disturbances [25]. For a step torque disturbance, ΔM_{dist} (at $t = 0$), the integrated position error can be reduced with higher $K_{i,\theta}$ as shown in (33) by applying the final value theorem on (31). However increasing $K_{i,\theta}$ also reduces the gain and phase margin. Finally the system inertia, J_{sys}, is compensated by the double-derivative gain, $K_{d2,\theta}$. This is proved by using the initial value theorem on (30) which consequently results in (34). The quantification of the feedback gains is explained next under the stability analysis.

$$L(j\omega) = \frac{K_{p,\theta} + j\omega(K_{p,\theta}T_f + K_{d,\theta})}{-(b_{sys}T_f + J_{sys})\omega^2 + j\omega(b_{sys} - J_{sys}T_f\omega^2)} \tag{32}$$

$$\lim_{t\to\infty}\int_0^t \Delta\theta_{mot}dt = \lim_{s\to 0}\frac{1}{s}\frac{\Delta\theta_{mot}(s)}{M_{dist}(s)}\Delta M_{dist} = \frac{-\Delta M_{dist}}{K_{i,\theta}} \tag{33}$$

$$\Delta\theta_{mot} = \lim_{s\to\infty}\frac{\Delta\theta_{mot}(s)}{\Delta\theta_{mot,ref}(s)}\Delta\theta_{mot,ref} = \frac{\Delta\theta_{mot,ref}}{1 + \frac{J_{sys}}{K_{d2,\theta}}} \tag{34}$$

The first step is to derive the inner loop stability criteria using (35) as the loop transfer function. The control law does not include the filter as simplification. As a necessary and sufficient stability condition, the constraint (36) must be satisfied. This result has been verified numerically and holds true for a stiff torsion bar. With decreasing c_{tb}, $K_{i,\theta}$ upper bound increases marginally. Equation (21) in torque control highlights that both $K_{i,M}$ and $K_{p,M}$ can be increased

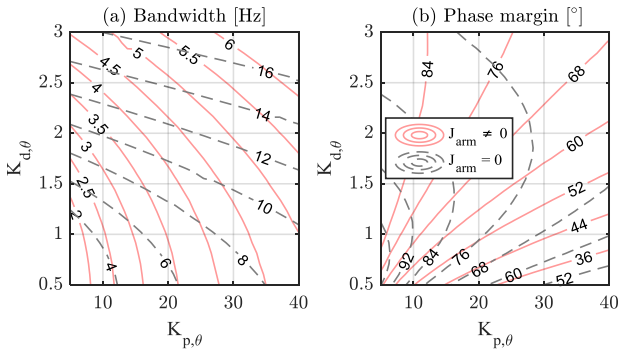

Fig. 5. The effect of position feedback control gains ($K_{p,\theta}$ and $K_{d,\theta}$) on (a) bandwidth and (b) loop gain phase margin are shown. The figures have been generated for $\{K_{i,\theta}, K_{d2,\theta}\} = 0$ and $T_f = 5$ms. Increasing $K_{p,\theta}$ ensures higher bandwidth but lower phase margin, whereas $K_{d,\theta}$ improves phase margin. Also, the bandwidth and phase margin reduces significantly with increasing driver arm inertia.

simultaneously (due to parabolic relation) to achieve tracking performance and compensate system inertia. Whereas in position control, the respective gains ($K_{i,\theta}$ and $K_{d2,\theta}$) fulfilling the same objectives exhibit hyperbolic relation for given $K_{p,\theta}$ and $K_{d,\theta}$. This is a key fundamental difference between the two approaches in terms of stability and performance. The feedback gains are chosen to provide 42° phase margin for (35) and approximately 5Hz position controller bandwidth with driver arm inertia. For the same controller gains without arm inertia, the phase margin and bandwidth are 75° and 10Hz respectively. The effect of J_{arm} variation on controller bandwidth can be seen in Fig. 4(b).

$$L_{in,\theta} = G_{Fb,\theta}\left|\frac{\theta_{mot}(s)}{M_{mot}(s)}\right|_{plant} \tag{35}$$

$$K_{i,\theta} < \left[\frac{b_s + b_{mot} + K_{d,\theta}}{J_s + J_{arm} + J_{mot} + K_{d2,\theta}}\right]K_{p,\theta} \tag{36}$$

Including the higher level control for stability evaluation requires the overall loop transfer function as shown in (37). The dependency on feedback gain $K_{d2,\theta}$ is limited since it would amplify the noise in angular acceleration error signal. Therefore the outer loop stability constraint is derived for the next higher order derivative, $K_{d,\theta}$. Considering a stiff torsion bar ($c_{tb} \to \infty$ and $k_{tb} = 0$), the outer loop is stable if $J_{ref} \geq J_{mot}$, $\forall\ K_{d,\theta} > 0$ as a sufficient condition for no loop gain encirclements of -1. This valid condition has been proved in [26]. However with known limited values of c_{tb} and k_{tb}, the quadratic constraint (38) on $K_{d,\theta}$ must be satisfied as a necessary and sufficient stability condition for LHP closed-loop poles of the characteristic equation. The derivation includes reasonable assumptions, $\{c_{ref}, b_{ref}, b_s, b_{mot}, K_{i,\theta}, K_{p,\theta}, K_{d2,\theta}\} = 0$. The desired $K_{d,\theta}$ bounds depend primarily on torsion bar parameters and inertia values. Equation (38) can also hold for $J_{ref} < J_{mot}$ for a certain $K_{d,\theta}$ range. This constraint is especially important for systems with indirect servo motor coupling because then the effective motor inertia on the torsion bar output shaft

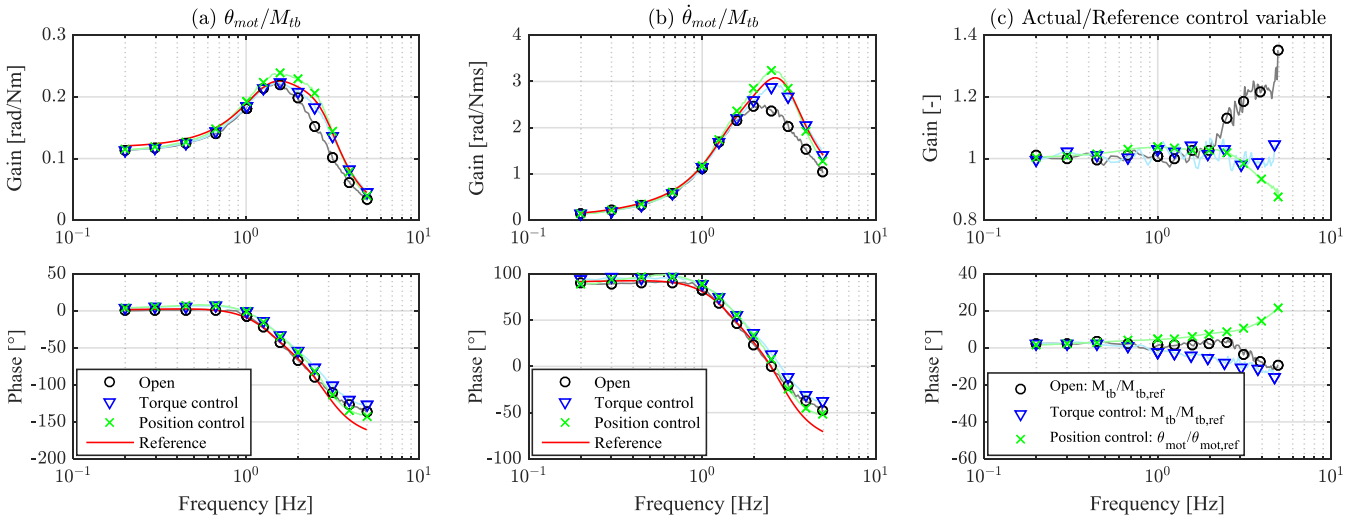

Fig. 6. Post-processed measurement data for performance evaluation. Frequency response of torsion bar torque to (a) feedback motor angle and (b) angular velocity with driver as an excitation source (open loop, torque and position control architectures). (c) Frequency response of reference haptic feedback function exhibiting the relation of reference to actual control variable. The closed-loop controllers offer a better response as compared to the open loop method as evident from reference tracking, especially in motor angular velocity response at higher frequencies ($>$ 2Hz).

increases incredibly, for example in EPAS system. For the given higher level control $J_{ref} >> J_{mot}$, so the outer loop remains stable $\forall\ K_{d,\theta} > 0$. But the inner loop constraint (36) creates a lower bound on $K_{d,\theta}$ to ensure controller stability for given $K_{i,\theta}, K_{p,\theta}$ and $K_{d2,\theta}$. The selected controller gains with reference parameters provide 75° phase margin for (37).

$$L_{o,\theta} = G_{Fb,\theta}\left[\left|\frac{\theta_{mot}(s)}{M_{mot}(s)}\right|_{plant} - G_{ref}\left|\frac{M_{tb}(s)}{M_{mot}(s)}\right|_{plant}\right] \tag{37}$$

$$K_{d,\theta}^2 + \left[\frac{\left(1-\frac{J_{mot}}{J_{ref}}\right)\frac{c_{tb}}{k_{tb}}}{\frac{1}{J_s+J_{arm}}+\frac{1}{J_{ref}}} + k_{tb}\left(1+\frac{J_{mot}}{J_s+J_{arm}}\right)\right]K_{d,\theta} + c_{tb}\frac{\left(\frac{J_{mot}}{J_s+J_{arm}}+1\right)^2}{\frac{1}{J_s+J_{arm}}+\frac{1}{J_{ref}}} > 0 \tag{38}$$

Lastly, the coupled haptic controller stability is evaluated. The effect of J_{arm} variation, as shown earlier in Fig. 4(b), significantly changes the controller bandwidth and subsequently inner- and outer-loop phase margins. The effect of muscle co-contraction, c_{arm}, variation on closed-loop steering admittance can be seen in Fig. 4(c). Contact stability is maintained since the phase margin of the loop transfer function (24) is positive. It implies positive real steering admittance, as the closed-loop poles remain in LHP.

The practical implementation of the designed control law ensured stability during experiments (both hands-off and rigidly coupled hands-on). Reference tracking of torsion bar torque to motor angle and angular velocity is improved as compared to the open loop, but inferior to the torque control approach as shown in Fig. 6(a) and (b) respectively. The position controller bandwidth is very much dependent on the driver arm inertia. Therefore, the reference haptic feedback function starts to deviate at higher frequencies (within excitation range), refer Fig. 6(c). As a result the tracking performance is somewhat compromised. Moreover, if an estimated torque signal for the higher level control is available, then this approach could be preferred by removing the torque sensor since the inner loop stability is roughly independent of it.

IV. CONCLUSIONS

This paper has presented a quantified comparison between the open and closed-loop haptic feedback control methods for Steer-by-Wire (SbW) systems. Although the open loop architecture is straightforward, but it lacks tracking performance at higher steering excitation frequencies due to feedback motor impedance. With a closed-loop solution, torque or position control, the effect of motor dynamics is compensated as shown in the experimental results.

In torque control, higher controller bandwidth is achieved as compared to position control. Because the closed-loop stability and performance are less sensitive to the driver arm inertia in torque control; whereas they reduce more rapidly with increasing inertia in position control. The haptic feedback control objectives are reference tracking and inertia compensation. Using classical control theory and linear stability analysis, it is proved that the two responsible feedback controller gains (corresponding to their respective objectives) show parabolic and hyperbolic constraint for torque and position control respectively. Also, torque control requires filtering for the reference generator which subsequently limits the reference tracking performance. On the contrary, filtering required for the position feedback control limits the controller performance (or bandwidth) and stability. For the controller design, the stability criteria have been derived and followed ensuring contact/coupled stability with the driver irrespective of the muscle co-contraction level. Finally, the experimental results corroborate the theoretical findings and stability criteria. The results show a comparable reference

tracking for torque and position control methods within driver's steering excitation range.

The authors intend to improve the position controller performance by compensating the driver arm inertia in the future. Also, the estimation and inclusion of the external road feedback in different haptic feedback control strategies will be further studied.

ACKNOWLEDGMENT

The authors would like to thank Professor Bengt Jacobson from Chalmers University of Technology and Pontus Carlsson, David Dahlgren and Joakim Norrby from Volvo Car Corporation for insightful discussions.

REFERENCES

[1] D. Gualino and I. J. Adounkpe, "Force-feedback system design for the steer-by-wire: optimisation and performance evaluation," in Proc. IEEE Intelligent Transp. Syst. Conf., Toronto, Canada, pp. 181-187, Sep. 2006.

[2] E. Mehdizadeh, M. Kabganian, and R. Kazemi, "A new force feedback for steer-by-wire vehicles via virtual vehicle concept," in Proc. 50th IEEE Conf. Dec. & Cont. & Eur. Cont. Conf., Orlando, USA, pp. 2281-2286, Dec. 2011.

[3] H. Hsu, M. Harrer, S. Grüner, and A. Gaedke, "The new steering system in the 911 porsche carrera - optimized design of a steering system for sportcars," in Proc. 21st Aachen Colloquium Auto. & Eng. Tech., 2012, pp. 633-647.

[4] M. Bröcker, "New control algorithms for steering feel improvements of an electric powered steering system with belt drive," Veh. Syst. Dyn., vol. 44, no. sup1, 2006, pp. 759-769.

[5] S. Fankem and S. Müller, "A new model to compute the desired steering torque for steer-by-wire vehicles and driving simulators," Veh. Syst. Dyn., vol. 52, no. sup1, 2014, pp. 251-271.

[6] A. Balachandran and J. C. Gerdes, "Designing steering feel for steer-by-wire vehicles using objective measures," IEEE/ASME Trans. Mech., vol. 20, no. 1, pp. 373-383, Feb. 2015.

[7] D. Camorali, G. Magnani, P. Rocco, and A. Rusconi, "Position/torque control of a space robotics arm," in Proc. 4th IFAC Symp. Mech. Syst., vol. 39, no. 16, 2006, pp. 283-288.

[8] E. de Vlugt, A. C. Schouten, F. C. T. van der Helm, P. C. Teerhuis, and G. G. Brouwn, "A force controlled planar haptic manipulator for posture control analysis of the human arm," J. Neurosci. Methods, vol. 129, no. 2, 2003, pp. 151-168.

[9] G. Ferretti, G. A. Magnani, P. Rocco, L. Vigano, and A. Rusconi, "On the use of torque sensors in a space robotics application," in Proc. IEEE/RSJ Int. Conf. Intelligent Rob. and Syst., 2005, pp. 1947-1952.

[10] C. Ott, R. Mukherjee, and Y. Nakamura, "Unified impedance and admittance control," in Proc. IEEE Int. Conf. Rob. & Aut., pp. 554-561, May 2010.

[11] A. C. Schouten, E. de Vlugt, J. J. B. van Hilten, and F. C. T. van der Helm, "Design of a torque-controlled manipulator to analyse the admittance of the wrist joint," J. Neuroscience Methods, vol. 154, no. 1, 2006, pp. 134-141.

[12] D. Katzourakis, D. Abbink, R. Happee, and E. Holweg, "Steering force-feedback for human-machine-interface automotive experiments," IEEE Trans. Instrum. Meas., vol. 60, no. 1, pp. 2303-2314, Jan. 2011.

[13] V. Lampaert, J. Swevers, and J. De Schutter, "Impact of nonlinear friction on frequency response function measurements," in Proc. Int. Conf. Noise & Vib. Engg., Leuven, Belgium, pp. 443-450, Sep. 2000.

[14] D. J. Cole, "A path-following driver-vehicle model with neuromuscular dynamics, including measured and simulated responses to a step in steering angle overlay," Veh. Syst. Dyn., vol. 50, no. 4, 2012, pp. 573-596.

[15] B. Lauber, M. Keller, C. Leukel, A. Gollhofer, and W. Taube, "Force and position control in humans - the role of augmented feedback," J. Vis. Exp. (112), Jun. 2016.

[16] L. Ljung, System Identification (2nd ed.): Theory for the User. Prentice Hall PTR, Upper Saddle River, NJ, USA, 1999, p. 168-189.

[17] M. Harrer and P. Pfeffer, Steering Handbook, Springer International Publishing, Switzerland, 2017, p. 163, 458-459.

[18] T. Chugh, F. Bruzelius, M. Klomp and S. Ran, "Comparison of steering feel control strategies in electric power assisted steering," presented at the 14th Int. Symp. on Advanced Vehicle Control (AVEC), Beijing, China, Jul. 2018.

[19] D. I. Katzourakis, D. A. Abbink, E. Velenis, E. Holweg, and R. Happee, "Driver's arms' time-variant neuromuscular admittance during real car test-track driving," IEEE Trans. Instrum. Meas., vol. 63, no. 1, pp. 221-230, Jan. 2014.

[20] R. Rajamani, Vehicle Dynamics and Control, Springer, New York, 2012, p. 27-40.

[21] M. V. Groll , S. Müeller , T. Meister and R. Tracht, "Disturbance compensation with a torque controllable steering system," Veh. Syst. Dyn., vol. 44, no. 4, 2006, pp. 327-338.

[22] K. J. Åström and R. M. Murray, Feedback Systems: An Introduction for Scientists and Engineers, Princeton University Press, Princeton and Oxford, 2010. p. 251-252, 284-289.

[23] E. Colgate and N. Hogan, "An analysis of contact instability in terms of passive physical equivalents," in Proc. Int. Conf. Rob. and Aut., vol. 1, pp. 404-409, 1989.

[24] J. E. Colgate and N. Hogan, "Robust control of dynamically interacting systems," Int. J. Control, vol. 48, no. 1, pp. 65-88, 1988.

[25] L. Harnefors, S. E. Saarakkala, and M. Hinkkanen, "Speed control of electrical drives using classical control methods," IEEE Trans. Ind. App., vol. 49, no. 2, pp. 889-898, Apr. 2013.

[26] G. Aguirre-Ollinger, J. E. Colgate, M. A. Peshkin and A. Goswami, "Design of an active one-degree-of-freedom lower-limb exoskeleton with inertia compensation," Int. J. Robotics Research, vol. 30, no. 4, 2011, pp. 486-499.